Beyer, C., Rosenthal, A., Myhill, R., Crichton, W. A., Yu, T., Wang, Y., & Frost, D. (2018). An internally consistent pressure calibration of geobarometers applicable to the Earth's upper mantle using in situ XRD. *Geochimica et Cosmochimica Acta*, *222*, 421-435. https://doi.org/10.1016/j.gca.2017.10.031

GCA 10536
7 November 2017
ARTICLE IN PRESS
No. of Pages 15

Available online at www.sciencedirect.com
ScienceDirect
Geochimica et Cosmochimica Acta xxx (2017) xxx–xxx
Geochimica et Cosmochimica Acta
www.elsevier.com/locate/gca

An internally consistent pressure calibration of geobarometers applicable to the Earth's upper mantle using *in situ* XRD

Christopher Beyer [a,b,*], Anja Rosenthal [c,d], Robert Myhill [e], Wilson A. Crichton [f], Tony Yu [g], Yanbin Wang [g], Daniel J. Frost [a]

[a] *Bayerisches Geoinstitut, Universität Bayreuth, 95440 Bayreuth, Germany*
[b] *Institut für Geologie, Mineralogie und Geophysik, Ruhr-Universität Bochum, 44780 Bochum, Germany*
[c] *Institute of Petrology and Structural Geology, Charles University in Prague, Albertov 6, 12843 Prague, Czech Republic*
[d] *Laboratoire Magmas et Volcans, Université Blaise Pascal – CNRS – IRD, OPGC, Campus Universitaire des Cézeaux, 6 Avenue Blaise Pascal, 63178 Aubière Cedex, France*
[e] *School of Earth Sciences, University of Bristol, Bristol BS8 1RJ, United Kingdom*
[f] *ESRF – The European Synchrotron, 71 avenue des Martyrs, 38000 Grenoble, France*
[g] *Center of Advanced Radiation Sources, The University of Chicago, 5460 S. Ellis Avenue, Chicago, IL, USA*

Received 9 February 2017; accepted in revised form 24 October 2017; available online xxxx

Abstract

We have performed an experimental cross calibration of a suite of mineral equilibria within mantle rock bulk compositions that are commonly used in geobarometry to determine the equilibration depths of upper mantle assemblages. Multiple barometers were compared simultaneously in experimental runs, where the pressure was determined using *in-situ* measurements of the unit cell volumes of MgO, NaCl, Re and h-BN between 3.6 and 10.4 GPa, and 1250 and 1500 °C. The experiments were performed in a large volume press (LVPs) in combination with synchrotron x ray diffraction. Noble metal capsules drilled with multiple sample chambers were loaded with a range of bulk compositions representative of peridotite, eclogite and pyroxenite lithologies. By this approach, we simultaneously calibrated the geobarometers applicable to different mantle lithologies under identical and well determined pressure and temperature conditions. We identified discrepancies between the calculated and experimental pressures for which we propose simple linear or constant correction factors to some of the previously published barometric equations. As a result, we establish internally-consistent cross-calibrations for a number of garnet-orthopyroxene, garnet-clinopyroxene, Ca-Tschermaks-in-clinopyroxene and majorite geobarometers.

Keywords: Geobarometry; Synchrotron; Multi-anvil; Calibration; Mantle; Eclogite; Peridotite

1. INTRODUCTION

Geobarometers are an essential tool for understanding geochemical and geodynamic processes of the Earth's interior. Their uses are manifold, ranging from the modelling of P-T paths of high-pressure rocks in mountain belts (e.g. Dale and Holland, 2003), the reconstruction of the chemical and thermal state of the lithosphere (Shirey et al., 2001; McKenzie et al., 2005; Smart et al., 2009) to the economic exploration of diamond-bearing rocks and the composition of the transition zone based on inclusions in diamonds (Walter et al., 2011). Geobarometers are routinely used to determine equilibration depths of mantle xenoliths

* Corresponding author at: Bayerisches Geoinstitut, Universität Bayreuth, 95440 Bayreuth, Germany.

https://doi.org/10.1016/j.gca.2017.10.031
0016-7037/© 2017 Published by Elsevier Ltd.

(Brey et al., 1990; Simakov, 2008; Ashchepkov et al., 2010; Beyer et al., 2015) and have also been used to infer inclusion formation depths in diamonds (Collerson et al., 2010; Wijbrans et al., 2016; Beyer and Frost, 2017). The majority of barometers used on mantle rocks have been calibrated using experiments where sample pressures have been previously calibrated using known high pressure mineral transformations or equilibria. Although the procedures and the transformations employed to calibrate high pressure apparatuses are well established and use transformations such as quartz – coesite (e.g. Bohlen and Boettcher, 1982), and fayalite – ringwoodite (see review in Keppler and Frost, 2005; Holloway and Wood, 2012), these *ex-situ* calibrations have uncertainties propagated from the method used to initially determine the transformation pressure and related to the reproducibility in pressure determination during the barometer calibration. This could potentially result in differences between apparent pressures determined by different barometer equilibria for rocks that came in fact from the same depth. Uncertainties in pressure determinations for calibration reactions arise from the fact that once frictional corrections for high pressure assemblies become necessary, absolute pressure determinations quite often rely on assumptions concerning equation of state measurements employed and the effect of thermal pressure. The reasons for poor pressure reproducibility are multifarious, and include for example, differences in the mode of piston operation in the piston-cylinder apparatus (Bose and Ganguly, 1995), differences in friction corrections of pressure cells (Bohlen and Boettcher, 1982), drift in the oil pressure vs. sample pressure in the multi-anvil apparatus over time and with changing temperature, differences in transformation volume changes and in the assembly design. Furthermore, there is the additional, although probably small uncertainly arising from the pressure effect on the thermocouple emf (Getting and Kennedy, 1970; Rubie, 1999). Some identified inter-laboratory discrepancies, for example, are lacking a plausible explanation, such as the 0.15 GPa difference between the quartz-coesite transition in "friction-free" NaCl cells of Bohlen and Boettcher (1982) and Bose and Ganguly (1995).

Here, we take a more rigorous approach and compare pressures calculated from the equation of states of widely used X-ray diffraction standard materials (Morard et al., 2007; Sokolova et al., 2016) directly with pressures obtained from a series of barometer equilibria, which are applicable to xenoliths and inclusions in diamonds from Earth's upper mantle (Brey et al., 1990, 2008; Simakov and Taylor, 2000; Simakov, 2008; Collerson et al., 2010; Beyer et al., 2015; Wijbrans et al., 2016; Beyer and Frost, 2017). Multi-chamber capsules, filled with various typical mantle bulk compositions, were employed in order to test a number of geobarometers in the same experiment under equivalent conditions. The multi-chamber capsule method has been successfully applied in several other studies where identical pressure and temperature conditions were essential (Liebske and Frost, 2012; Myhill et al., 2017). We compare the pressures calculated from the X-ray-determined unit-cell volumes of the pressure standards with the pressures estimated from the geobarometer equilibria and propose corrections, where necessary. The resulting directly comparable calibrations should give confidence in the application of different geobarometers to the same suite of rocks and should yield mutually consistent depths of last equilibration.

2. METHODS

2.1. Starting materials

A series of bulk compositions were selected to cover the most common mantle lithologies with mafic and ultramafic compositions (Table 1). NMORB4 (Beyer and Frost, 2017) and Mix-1G (Hirschmann et al., 2003) are synthetic glasses with normal hydrous mid-ocean ridge basalt (MORB) and pyroxenitic compositions respectively. Details on the fabrication of the glasses are given in Beyer and Frost (2017). KLB-1 is a fused glass that represents a synthetic spinel lherzolite (Takahashi, 1986), whereas KLB-1n is a simplified synthetic harzburgite glass (Walter, 1998), being more refractory (higher Mg#) and containing no Na_2O relative to KLB-1 (Table 1). Both glasses were synthesized at 1600 °C in a 1-atm furnace for 90 min. The peridotitic glasses contain µm-sized phenocrystals that crystallize unavoidably during quenching. We also conducted experiments using a synthetic average altered MORB composition, GA20, which is similar to GA2 (Spandler et al., 2008) but with Cr_2O_3 and P_2O_5 removed. P2 is a fertile lherzolite oxide mix guided by the composition HZ-1, representative ofa MORB source (Green et al., 2010). Oxide powders of GA20 and P2 were prepared using established procedures (Green et al., 2010; Rosenthal et al., 2014). Ir was added as IrO_2 to both GA20 and P2 to act as a redox sensor, however, due to the small size of the resulting alloy and due to mixing with Re we ultimately did not employ the sensor. Approximately 1 µl of distilled water was also added to the dry peridotitic compositions to promote equilibration.

2.2. Experimental methods

Experiments were performed at beamline ID06 of the European Synchrotron Radiation Facility, Grenoble, France using a 2000-tonne modified DIA press in 6/8 configuration and at the 13-ID-D beamline of GSECARS at the Advanced Photon Source, Argonne, Illinois, USA using a 1000-tonne press and a T-25 double-stage multi-anvil module (Wang et al., 2009). Experiments were conducted between pressures of 3.6 to 10.4 GPa at temperatures from 1200 to 1500 °C. An octahedron with 14 mm truncated edge length, made from semi-sintered Cr_2O_3-doped MgO, was compressed using 8 tungsten carbide anvils of 25 mm edge length and with 8 mm edge length corner truncations. The assembly was drilled for the insertion of a Re-foil furnace. The Re-foil (250 µm thickness, 99.995% purity) was modified with two opposing slits (0.5 × 2.7 mm) for unimpeded X-ray transmission. The furnace was enclosed within a cylindrical sleeve of MgO or h-BN at the center of the assembly and a ZrO_2 sleeve above and below the beam path (Fig. 1b). For the experiments performed at ESRF, parts of

Please cite this article in press as: Beyer C., et al. An internally consistent pressure calibration of geobarometers applicable to the Earth's upper mantle using *in situ* XRD. *Geochim. Cosmochim. Acta* (2017), https://doi.org/10.1016/j.gca.2017.10.031

Table 1
Compositions of starting materials in wt.% oxides.

	NMORB4	GA20	Mix-1G	P2	KLB-1n	KLB-1
SiO_2	50.5	46.3	45.56	44.66	39.4	44.5
TiO_2	2.8	0.89	0.9	0.17		0.16
Al_2O_3	13.2	19.0	15.19	3.94	2.0	3.59
Cr_2O_3				0.39		0.31
FeO[a]	9.6	10.48	7.77	7.34	5.2	8.1
NiO				0.27		
MnO		0.14	0.15	0.10		0.12
MgO	6.1	11.59	16.67	36.70	49.5	39.22
CaO	11.5	9.24	11.48	3.12	3.3	3.44
Na_2O	2.8	2.33	1.44	0.32		0.3
K_2O	0.4		0.04	0.03		
H_2O	3		2			
IrO_2				2.91		
Total	99.9	100.0	101.2	100.0	99.4	99.7

[a] Total Fe.

the octahedron were replaced with boron-epoxy to enable better X-ray transmission (Fig. 1a). Mo electrodes on each side of the furnace ensured good electrical contact with the tungsten carbide cubes. The temperature was monitored with an axially inserted D-type thermocouple (W_3Re–$W_{25}Re$) in proximity to the multi-chamber capsule. In order to minimize the uncertainty from temperature measurements, X-ray diffraction patterns were collected next to the thermocouple junction and the sample capsule. The location of the target sample region with respect to the X-ray beam was monitored using in-line X-ray radiography. The electrical power to the furnace was manually controlled with a Eurotherm temperature controller.

In each experiment four different starting powders were loaded into 0.25 mm wide and 0.6 mm deep chambers that were spark-eroded into discs machined from Re or $Au_{80}Pd_{20}$ with 1.6 mm diameter and 0.8 mm height. Capsules were covered with a 0.2 mm thick Re or $Au_{80}Pd_{20}$ disc, which cold sealed the capsule chambers during compression.

About 0.3 mm thick layers of X-ray calibrant powders were placed above and below the capsule to ensure that an X-ray standard was always within the anvil gap region that is accessible to x ray diffraction. Mixtures of MgO + h-BN (1:4), MgO + Pt (15:1), NaCl + Au (10:1), were chosen as X-ray standards based on their melting points and their well-determined thermal equations of state and additionally that the mixture of ceramic and metal ensured suitable accuracy in the estimation of both temperature and pressure in cases where there was a loss of the thermocouple. The use of mixed standards also partly inhibits the formation of large gains by pinning the growth of grain boundaries, which would otherwise result in poor diffraction statistics. At ESRF, Re from the furnace and h-BN from the sleeve around the sample capsule were used to cross-calibrate and further improve the precision of the calculated pressures (Crichton and Mezouar, 2002; Morard et al., 2007). These measurements required the collection of angle-dispersive X-ray diffraction data, on a linear pixelated GOS X-scan series detector from Detection Technology, through the horizontal anvil gap. For this we used a monochromatic beam of wavelength, $\lambda = 0.2254$ Å (55 keV), which was selected from the emission of a U18 undulator by a Cinel Si(111) double-crystal monochromator. The unfocussed incident beam size was 0.5 mm × 0.5 mm. The detector ran continuously, collecting a new image at 10 Hz rate and writing images to disk every 3.2 s. The 3.2 s detector images were integrated using v17 of Fit2D (Hammersley, 2016) after correction according to the detector's location on the calibrated X-ray detector plane, which was at approximately 2050 mm from the sample.

At APS energy-dispersive powder X-ray diffraction patterns were recorded using a Ge solid-state detector at a fixed diffraction angle (2Θ) of ~6°. Energies were calibrated using the weighted average of Ag Kα1 and Kα2 (22.104 keV), Ag Kβ1 (24.942 keV), the γ lines of Cd^{109} (88.040 keV) and Co^{57} (122.061 keV). The incident beam was collimated to 0.2 × 0.2 mm^2, and the diffracted beam size was approximately the same. Typical uncertainties in energy calibration are <10 eV.

Experiments were pressurized at room temperature and then heated to ~450 °C for 1 h to release residual stress from the cold compression. Afterwards the experiments were cooled to room temperature and subsequently heated to the final run temperature over 15–20 min. The temperature was kept constant for several hours (Table 1). Subsequently, experiments were quenched by shutting off the power causing a drop to <100 °C within ~10 s. Recovered capsules were embedded into epoxy resin, sectioned and polished with a series of SiC grinding papers and diamond paste. Run products were examined by reflected light microscopy, and then carbon-coated for microbeam analyses.

2.3. Analytical methods

Experimental charges were examined qualitatively using secondary and back-scattered electron imaging on a Zeiss Gemini 1530 scanning electron microscope (SEM) equipped with a field-emission gun. Quantitative analyses

Please cite this article in press as: Beyer C., et al. An internally consistent pressure calibration of geobarometers applicable to the Earth's upper mantle using *in situ* XRD. *Geochim. Cosmochim. Acta* (2017), https://doi.org/10.1016/j.gca.2017.10.031

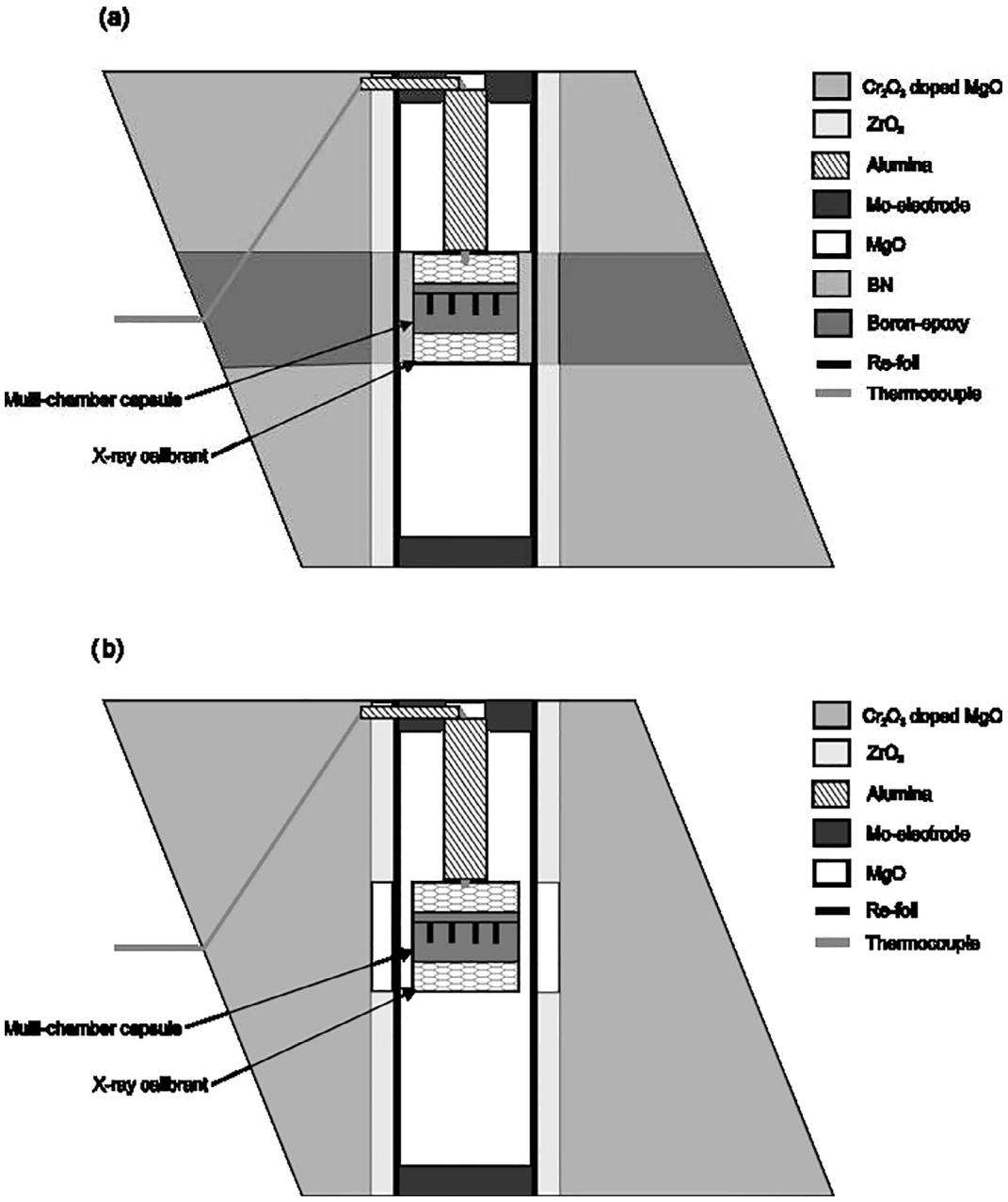

Fig. 1. Cross-sections of the high-pressure assemblies used for experiments at (a) ESRF and (b) APS. The height of each assembly is 11 mm.

of coexisting phases were carried out using a JEOL JXA 8200 installed at the Bayerisches Geoinstitut Bayreuth and a JEOL 8350F equipped with a field-emission gun installed at the University of Münster. Both microprobes were operated at 15 kV with a 15 nA beam current. Phases were analyzed using a focused beam on the JEOL JXA 8200, whereas, a 3 μm defocused beam was used on the JEOL 8350F to excite a comparable sample volume. In order to obtain accurate analyses, matrix-matched mineral standards were used (K, anorthite; Na, jadeite; Ca, diopside/grossular; Mg, diopside/pyrope; Mn, $MnTiO_3$/rutile; Fe, Fe-metal/almandine; Cr, Cr-metal; Al, jadeite/pyrope; Ti, rutile; Si, diopside/pyrope). Having separate garnet and pyroxene standards for major element analyses of these minerals significantly improved the analyses of these elements and particularly Si. To make certain that the analyses were not biased by using two different microprobes, some arbitrarily selected garnets and pyroxenes were measured with both machines. The analyses agreed within the statistical uncertainties of the measurements (Table 4).

The zero pressure volumes of the calibrants were collected for each experiment and used as a reference volume for the equation of state (EoS) fitting procedure. EDX patterns were converted using the software PDIndexer (Seto et al., 2010), whereas ADX patterns were treated using Fit2D. The unit-cell volumes were calculated with a mini-

Please cite this article in press as: Beyer C., et al. An internally consistent pressure calibration of geobarometers applicable to the Earth's upper mantle using *in situ* XRD. *Geochim. Cosmochim. Acta* (2017), https://doi.org/10.1016/j.gca.2017.10.031

mum of three indexed diffraction peaks for each diffraction pattern. w. The mean variance of the lattice parameters provides an estimate of the uncertainty on the unit-cell volume. The data treatment and pressure calculation is described in the next section in greater detail.

3. RESULTS AND DISCUSSION

Experimental run conditions are given in Table 2. Recovered samples yielded euhedral to subhedral crystals and a small fraction of quenched melt was identified in some runs. Despite the addition of water to the peridotitic compositions, no hydrous phases were found in the experiments, in agreement with their reported stability fields (Green et al., 2010).

Chemical analyses for garnets and pyroxenes are reported in Tables 3 and 4. All capsule chambers that are not given in Table 2 were excluded on the basis that they showed a poor degree of equilibration, i.e. strong zonation in the BSE-images, dendritic cores rich in inclusions and large chemical variation between grains. Only samples where microprobe analysis totals were between 98.5 wt.% and 101.5 wt.% were used for further analyses. In starting materials where IrO_2 was added (NMORB4, P2, GA20), 1–5 μm sized nuggets of IrFe-alloy were distributed randomly throughout the capsules and were preferentially found on grain boundaries. Hydrous samples showed no evidence for excess fluid being present, such as bubbles within the melt phase or highly porous aggregates, therefore, we assume that any water was principally dissolved in the melt, with a small amount also partitioned into minerals (Katayama et al., 2003; Hirschmann et al., 2005).

3.1. Eclogites and pyroxenites

Experiments on eclogitic bulk compositions (NMORB4, GA20) contain garnet, clinopyroxene, and coesite/stishovite (Fig. 2a). Subordinate quenched melt pockets are present in sample ES313-2 (GA20). Run products from the pyroxenitic starting material Mix-1G yielded a bimineralic assembly with euhedral garnet and xenomorphic clinopyroxene. Garnet grains show a euhedral crystal habit and are generally homogeneous. In some experiments, garnet is slightly compositionally zoned, exhibiting Ca-, Al-, and Fe-rich cores. In these cases, only rim analyses were considered, as they are inferred to have more closely approached chemical equilibrium with the surrounding phases. Garnets with unusual "patchy" textures in some of the runs were neglected from further analyses. Garnets at pressures below 5.6 GPa are solid solutions mostly consisting of pyrope ($Mg_3Al_2Si_3O_{12}$, 0.24–0.71 mol), almandine ($Fe_3Al_2Si_3O_{12}$, 0.05–0.32 mol), grossular ($Ca_3Al_2Si_3O_{12}$, 0.24–0.37 mol) and trace amounts of Mn, Na, and Ti. The majoritic garnet components, $Mg_3(MgSi)Si_3O_{12}$ and $Na_2Mg(Si_2)Si_3O_{12}$, were only observed at pressures above 5 GPa. The majorite content reached a maximum concentration of 0.150 mol at pressures of 9.4(2) GPa in sample ES313-5-1. The sodium-bearing component dominants the majoritic substitution in eclogitic compositions, whereas, the Mg-Si majorite component dominants in pyroxenitic bulk compositions.

Clinopyroxenes formed as homogenous subhedral crystals. No evidence for compositional zoning was observed during microbeam transect analyses performed from cores to rims. All clinopyroxenes have omphacitic compositions. For the silica-saturated eclogites NMORB4 and GA20, the major clinopyroxene components are jadeite, diopside-hedenbergite, enstatite-ferrosilite, Ca-Tschermaks, Ca-Eskolaite, with minor amounts of Ti and K, which is similar to previous eclogite studies (Irifune et al., 1986; Spandler et al., 2008; Beyer et al., 2015; Rosenthal et al., 2015). With increasing pressure, the jadeite content increases, while Ca-Tschermaks, diopside and hedenbergite components decrease.

3.2. Peridotites

Experiments on peridotitic bulk starting materials (P2, KLB-1, KLB-1n) yielded garnets, orthopyroxenes, olivines and occasional clinopyroxene (Fig. 2b, Table 2). Despite the addition of H_2O to the peridotitic starting powders to act as a flux, only approximately half of the experiments crystallized homogeneous peridotitic mineral phases that were suitable for further calculations. At temperatures <1300 °C, run products of P2 approached equilibrium conditions only in one experiment. We assume that the duration of P2 experiments at lower temperatures was too short to promote the attainment of equilibrium of the phase assemblage. Run products from capsule chambers filled

Table 2
Experimental conditions.

Run	Calibrant	Time [h]	P [GPa]	T [°C]	Capsule	Starting materials
APS						
T1744	MgO	3	5.6(3)	1400(10)	Re	**NMORB4**, Mix-1G, **P2**, KLB-1
T1746	MgO	3	8.0(3)	1400(15)	Re	**NMORB4**, **Mix-1G**, P2, **KLB-1**
T1748	MgO	2	10.4(2)	1500(15)	Re	**NMORB4**, Mix-1G, **P2**, KLB-1
ESRF						
ES313-1	Re,h-BN	8	4.3(2)	1293(30)[a]	$Au_{80}Pd_{20}$	**NMORB4**, GA20, **KLB-1n**, P2
ES313-2	Re,h-BN	6	5.5(2)	1300(10)	$Au_{80}Pd_{20}$	**NMORB4**, **GA20**, **KLB-1n**, P2
ES313-4	Re,h-BN	14 ½	3.6(1)	1250(10)	$Au_{80}Pd_{20}$	**NMORB4**, **GA20**, **KLB-1n**, **P2**
ES313-5	NaCl	18	9.4(2)	1400(10)	$Au_{80}Pd_{20}$	**NMORB4**, GA20, KLB-1n, P2

Bold experiments approached equilibrium.
[a] Based on Re, h-BN cross calibration.

Please cite this article in press as: Beyer C., et al. An internally consistent pressure calibration of geobarometers applicable to the Earth's upper mantle using *in situ* XRD. *Geochim. Cosmochim. Acta* (2017), https://doi.org/10.1016/j.gca.2017.10.031

Table 3
Garnet compositions based on EMPA analyses in wt.% oxides.

	T1744-1	1σ	T1744-3	1σ	T1746-1	1σ	T1746-2	1σ	T1746-3	1σ	T1746-4	1σ
n	7		5		11		10		16		7	
SiO_2	**40.10**	0.3	**42.4**	0.3	**40.3**	0.2	**42.0**	0.2	**43.46**	0.17	**42.7**	0.3
TiO_2	**1.26**	0.2	**0.2**	0.1	**1.3**	0.1	**0.6**	0.2	**0.31**	0.06	**0.39**	0.03
Al_2O_3	**21.72**	0.3	**21.9**	0.3	**21.6**	0.2	**21.9**	0.4	**20.9**	0.2	**20.3**	0.2
Cr_2O_3	**b.d.l.**		**1.6**	0.3	**b.d.l.**		**b.d.l.**		**1.86**	0.09	**1.0**	0.1
FeO	**14.93**	0.08	**5.7**	0.3	**14.4**	0.1	**8.0**	0.4	**5.5**	0.1	**7.2**	0.1
MnO	**0.05**	0.03	**0.17**	0.04	**0.03**	0.02	**0.24**	0.04	**0.19**	0.02	**0.04**	0.03
MgO	**9.5**	0.2	**21.9**	0.3	**9.5**	0.2	**17.2**	0.4	**23.7**	0.2	**21.8**	0.6
CaO	**11.5**	0.3	**4.6**	0.4	**12.4**	0.2	**9.4**	0.8	**4.5**	0.3	**5.0**	0.6
Na_2O	**0.29**	0.03	**0.03**	0.02	**0.39**	0.03	**0.20**	0.03	**0.03**	0.01	**0.06**	0.01
K_2O	**0.02**	0.01	**b.d.l.**		**b.d.l.**		**b.d.l.**		**b.d.l.**		**b.d.l.**	
Total	99.3		98.6		100.0		99.61		100.52		98.54	

	T1748-1	1σ	T1748-3	1σ	ES313-1-1	1σ	ES313-1-3	1σ	ES313-2-1	1σ	ES313-2-2	1σ
n	12		6		4		18		11		18	
SiO_2	**40.7**	0.2	**44.9**	0.1	**41.6**	0.3	**43.5**	0.2	**40.7**	0.3	**41.0**	0.4
TiO_2	**1.2**	0.1	**0.4**	0.1	**1.2**	0.2	**0.09**	0.02	**1.2**	0.1	**1.14**	0.08
Al_2O_3	**21.0**	0.2	**18.8**	0.2	**23.0**	0.4	**24.03**	0.19	**22.0**	0.2	**22.8**	0.2
Cr_2O_3	**b.d.l.**		**1.3**	0.2	**b.d.l.**		**b.d.l.**		**b.d.l.**		**b.d.l.**	
FeO	**13.9**	0.1	**6.3**	0.1	**7.0**	1.0	**1.50**	0.25	**10.5**	0.4	**8.6**	0.8
MnO	**0.03**	0.03	**0.21**	0.04	**0.12**	0.04	**b.d.l.**		**0.10**	0.03	**0.27**	0.03
MgO	**9.5**	0.2	**24.1**	0.3	**14.6**	1.0	**24.43**	0.44	**11.0**	0.2	**13.9**	0.5
CaO	**13.0**	0.3	**3.8**	0.2	**12.7**	0.2	**5.46**	0.24	**13.9**	0.4	**11.0**	0.3
Na_2O	**0.55**	0.04	**0.10**	0.01	**0.22**	0.02	**b.d.l.**		**0.03**	0.01	**0.03**	0.01
K_2O	**b.d.l.**				**b.d.l.**				**0.01**	0.01	**0.01**	0.02
Total	99.81		99.93		**100.4**		**99.1**		**99.4**		**98.8**	

	ES313-4-3	1σ	ES313-4-4	1σ	ES313-5-1	1σ	ES313-2-3	1σ	ES313-4-1	1σ	ES313-4-2	1σ
n	16		12		7		7		11		7	
SiO_2	**43.6**	0.1	**43.0**	0.2	**40.5**	0.4	**43.6**	0.3	**42.6**	0.3	**42.8**	0.6
TiO_2	**b.d.l.**		**0.22**	0.03	**1.5**	0.2	**b.d.l.**		**0.73**	0.08	**0.75**	0.08
Al_2O_3	**24.3**	0.1	**22.7**	0.3	**20.4**	0.3	**23.6**	0.2	**23.7**	0.2	**23.8**	0.2
Cr_2O_3	**b.d.l.**		**1.74**	0.35	**0.01**	0.01	**b.d.l.**		**0.05**	0.03	**0.02**	0.01
FeO	**1.11**	0.05	**1.13**	0.04	**13.8**	0.3	**2.4**	0.2	**2.7**	0.2	**2.5**	0.2
MnO	**b.d.l.**		**0.19**	0.04	**0.06**	0.03	**0.07**	0.05	**0.24**	0.06	**0.29**	0.06
MgO	**24.8**	0.3	**24.06**	0.40	**8.9**	0.1	**24.2**	0.1	**18.9**	0.4	**19.7**	0.4
CaO	**5.3**	0.3	**5.89**	0.23	**13.5**	0.3	**5.1**	0.2	**10.5**	0.5	**9.3**	0.2
Na_2O	**b.d.l.**		**b.d.l.**		**0.06**	0.01	**0.01**	0.01	**0.01**	0.01	**0.01**	0.01
K_2O	**b.d.l.**		**b.d.l.**		**0.03**	0.01	**b.d.l.**		**0.01**	0.01	**0.01**	0.01
Total	**99.2**		**99.0**		**98.8**		**98.9**		**99.4**		**99.1**	

b.d.l.: below detection limit; n: number of analyses.

with KLB-1 were also generally poorly equilibrated. Only experiment T1746-4 yielded a compositionally homogeneous peridotitic phase assemblage. Therefore, in the subsequent experiments at ESRF, spinel lherzolite KLB-1 was replaced by the KLB-1n harzburgite composition. Experiments employing KLB-1n appeared to approach equilibrium and contained euhedral garnet, orthopyroxene, and olivine. Garnet solid solutions are comprised of between 0.75 to 0.85 mol fraction pyrope and subordinate amounts of almandine and grossular. The maximum proportion of majoritic garnet components was measured in T1748-3 at 10.4(3) GPa where the garnets contained ~3.15 Si per formula unit. Orthopyroxenes are enstatitic, with subordinate amounts of ferrosilite and diopside. The Mg# (Mg/Fe + Mg) ranges from 0.93 to 0.99. Olivines are close to the forsterite end-member, with Mg# = 0.90–0.99.

In some experiments (with high Mg#), Fe was lost to the $Au_{80}Pd_{20}$ capsule. To check if the samples approached equilibrium we compared the experimental temperature with the Ca-in-opx thermometer (Brey and Köhler, 1990). We found that the peridotitic samples were in very good agreement with $\Delta T_{max} = 60$ K and $\Delta T_{ave} = 40$ K. However, Al seems to have not reached equilibrium in orthopyroxene. We argue that Fe was lost during the initial stage of heating. Because Al and Fe are negatively correlated in orthopyroxene (Lee and Ganguly, 1988) the Al concentration has been altered as well. Taking into account the slow diffusivity of Al in orthopyroxene (Smith and Barron, 1991), Al has not reached equilibrium for the duration of

Please cite this article in press as: Beyer C., et al. An internally consistent pressure calibration of geobarometers applicable to the Earth's upper mantle using *in situ* XRD. *Geochim. Cosmochim. Acta* (2017), https://doi.org/10.1016/j.gca.2017.10.031

Table 4
Pyroxene compositions based on EMPA analyses in wt.% oxides.

	T1744-1	1σ	T1744-3	1σ	T1746-1	1σ	T1746-2	1σ	T1746-3	1σ
n	15		7		12		13		9	
SiO_2	**54.9**	0.5	**57.9**	0.2	**55.5**	0.2	**55.1**	0.3	**57.4**	0.2
TiO_2	**1.2**	0.2	**0.03**	0.01	**1.1**	0.1	**0.17**	0.03	**0.03**	0.03
Al_2O_3	**12.3**	0.2	**1.2**	0.1	**12.5**	0.2	**4.5**	0.3	**0.8**	0.1
Cr_2O_3			**0.18**	0.02					**0.13**	0.01
FeO	**4.8**	0.3	**4.6**	0.1	**4.7**	0.3	**3.2**	0.1	**4.3**	0.3
MnO	**0.01**	0.01	**0.09**	0.03	**0.02**	0.03	**0.06**	0.03	**0.09**	0.02
MgO	**8.4**	0.2	**34.1**	0.2	**7.9**	0.1	**15.7**	0.2	**34.5**	0.3
CaO	**13.6**	0.5	**1.7**	0.1	**12.6**	0.3	**19.2**	0.5	**1.5**	0.1
Na_2O	**5.1**	0.2	**0.14**	0.02	**6.0**	0.3	**2.5**	0.1	**0.15**	0.01
K_2O	**0.03**	0.01	**0.01**	0.01	**0.07**	0.02	**0.02**	0.01		
Total	**100.3**		**100.0**		**100.3**		**100.3**		**99.0**	

	T1746-4	1σ	T1748-1	1σ	T1748-3(opx)	1σ	T1748-3(cpx)	1σ	ES313-1-1	1σ
n	11		9		7		13		15	
SiO_2	**55.7**	0.3	**56.3**	0.4	**58.1**	0.1	**56.4**	0.4	**53.7**	0.1
TiO_2	**0.08**	0.02	**0.6**	0.1	**0.04**	0.01	**0.08**	0.05	**1.2**	0.1
Al_2O_3	**1.5**	0.1	**12.3**	0.6	**0.7**	0.1	**1.4**	0.2	**15.9**	0.2
Cr_2O_3	**0.18**	0.03	**0.01**	0.01	**0.14**	0.03	**0.26**	0.03		
FeO	**4.5**	0.1	**4.4**	0.3	**4.63**	0.03	**4.0**	0.2	**1.3**	0.3
MnO	**0.01**	0.02	**0.01**	0.01	**0.10**	0.02	**0.14**	0.03	**0.03**	0.02
MgO	**22.8**	0.5	**8.1**	0.5	**33.8**	0.4	**23.7**	0.5	**8.3**	0.1
CaO	**14.5**	0.4	**12.3**	0.5	**1.9**	0.5	**12.6**	0.4	**14.4**	0.1
Na_2O	**0.85**	0.03	**6.3**	0.4	**0.28**	0.03	**1.13**	0.16	**4.8**	0.1
K_2O			**0.08**	0.01					**0.011**	0.006
Total	**100.1**		**100.5**		**99.7**		**99.8**		**99.6**	

	ES313-1-3	1σ	ES313-2-1	1σ	ES313-2-2	1σ	ES313-2-3(opx)	1σ	ES313-2-3(cpx)	1σ
n	9		10		13		3		7	
SiO_2	**58.4**	0.2	**55.9**	0.6	**56.3**	0.4	**57.8**	0.6	**55.2**	0.2
TiO_2	**0.02**	0.02	**0.8**	0.1	**1.0**	0.2	**0.02**	0.02	**0.002**	0.004
Al_2O_3	**1.3**	0.1	**15.5**	0.7	**17.5**	0.5	**0.8**	0.0	**0.78**	0.04
Cr_2O_3	**0.01**	0.01					**0.01**	0.01	**0.01**	0.01
FeO	**1.3**	0.2	**2.3**	0.3	**2.0**	0.3	**1.7**	0.2	**1.5**	0.4
MnO			**0.03**	0.03	**0.04**	0.03	**b.d.l.**		**b.d.l.**	
MgO	**38.2**	0.3	**7.4**	0.4	**6.4**	0.4	**38.0**	0.6	**22.8**	0.3
CaO	**1.2**	0.1	**13.0**	0.6	**10.6**	0.4	**1.3**	0.1	**19.0**	0.6
Na_2O			**5.7**	0.4	**6.8**	0.5	**0.01**	0.01	**0.06**	0.01
K_2O			**b.d.l**		**0.0**	0.0				
Total	**100.4**		**100.6**		**100.7**		**99.6**		**99.3**	

	ES313-4-1	1σ	ES313-4-2	1σ	ES313-4-3(opx)	1σ	ES313-4-3(cpx)	1σ
n	7		9		8		6	
SiO_2	**53.2**	0.5	**53.7**	0.4	**58.8**	0.1	**55.7**	0.2
TiO_2	**1.2**	0.1	**1.3**	0.1	**0.01**	0.01	**0.01**	0.02
Al_2O_3	**15.6**	0.3	**16.3**	0.5	**1.7**	0.1	**1.5**	0.1
Cr_2O_3					**0.01**	0.01	**0.01**	0.01
FeO	**0.7**	0.2	**0.6**	0.1	**0.9**	0.1	**0.46**	0.03
MnO	**0.1**	0.0	**0.07**	0.02	**0.04**	0.02	**0.04**	0.02
MgO	**9.5**	0.3	**9.3**	0.4	**37.6**	0.2	**21.1**	0.3
CaO	**15.8**	0.7	**15.0**	0.5	**1.3**	0.1	**22.1**	0.5
Na_2O	**4.0**	0.3	**4.6**	0.4	**0.1**	0.1	**0.2**	0.2
K_2O	**0.02**	0.02	**0.01**	0.01				
Total	**100.2**		**100.8**		**100.4**		**101.0**	

(*continued on next page*)

Please cite this article in press as: Beyer C., et al. An internally consistent pressure calibration of geobarometers applicable to the Earth's upper mantle using *in situ* XRD. *Geochim. Cosmochim. Acta* (2017), https://doi.org/10.1016/j.gca.2017.10.031

Table 4 (*continued*)

	ES313-4-4 (opx)	1σ	ES313-4-4(cpx)	1σ	ES313-5-1	1σ
n	8		8		8	
SiO_2	**58.0**	0.1	**55.2**	0.3	**56.5**	0.6
TiO_2	**0.06**	0.02	**0.08**	0.02	**0.8**	0.2
Al_2O_3	**1.65**	0.05	**1.9**	0.1	**13.1**	0.4
Cr_2O_3	**0.23**	0.03	**0.5**	0.1		
FeO	**0.9**	0.1	**0.5**	0.2	**3.8**	0.1
MnO	**0.12**	0.03	**0.08**	0.04	**0.01**	0.01
MgO	**37.4**	0.1	**20.7**	0.2	**7.4**	0.2
CaO	**1.2**	0.1	**21.3**	0.6	**11.7**	0.2
Na_2O	**0.1**	0.1	**0.5**	0.2	**7.1**	0.3
K_2O					**0.21**	0.04
Total	**99.6**		**100.8**		**100.7**	

b.d.l.: below detection limit; n: number of analyses.

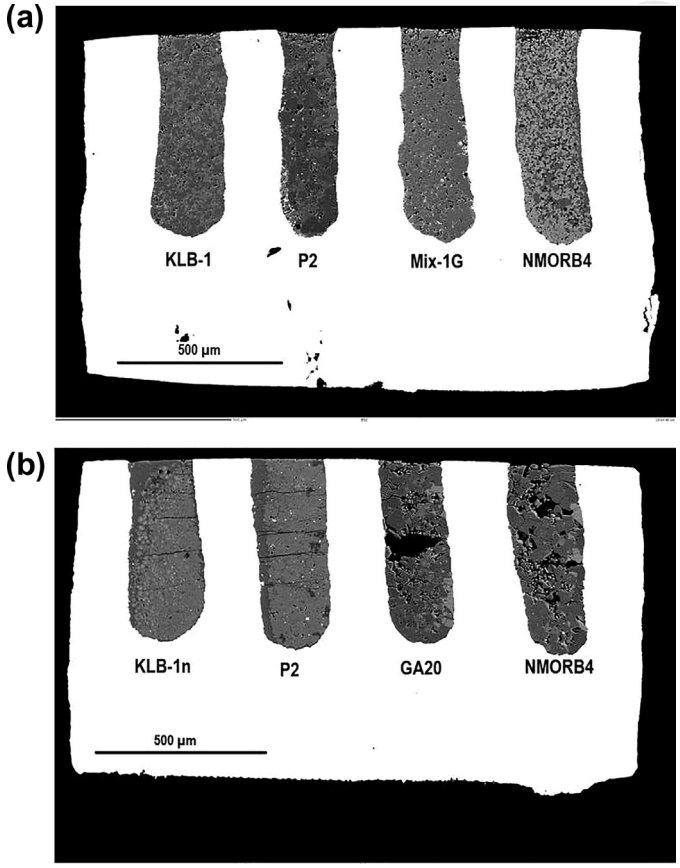

Fig. 2. Back-scattered electron images of two representative capsules of recovered experiments. (a) Run T1746 (8 GPa, 1400 °C, Re capsule). (b) Run ES313-4 (3.6 GPa, 1250 °C, $Au_{80}Pd_{20}$ capsule). Black areas within the capsule chambers are voids caused by broken out crystals.

the experiment. The consequences for Al-in-opx barometry will be discussed in the upcoming section on peridotitic barometers.

3.3. Pressure calibration

Calculated pressures are given in Table 1. Two representative diffraction patterns are shown in Fig. 3a/b. We employed the unit-cell volume of MgO, coupled with thermocouple temperatures, to calculate *in-situ* pressures using the third-order Birch-Murnaghan EoS combined with the modified Mie-Grüneisen-Debye formulation to calculate the thermal pressure (Tange et al., 2009) for experiments carried out at APS (T174x). The pressures of experiments conducted at ESRF were calculated using a cross-calibration of Re and h-BN lattice volumes for pressure (Le Godec et al., 2000; Zha et al., 2004) and temperature (ES313-1), due to thermocouple failure on compression, and from the EoS of the reference materials, coupled with the thermocouple temperature (ES313-2, ES313-4). For

Please cite this article in press as: Beyer C., et al. An internally consistent pressure calibration of geobarometers applicable to the Earth's upper mantle using *in situ* XRD. *Geochim. Cosmochim. Acta* (2017), https://doi.org/10.1016/j.gca.2017.10.031

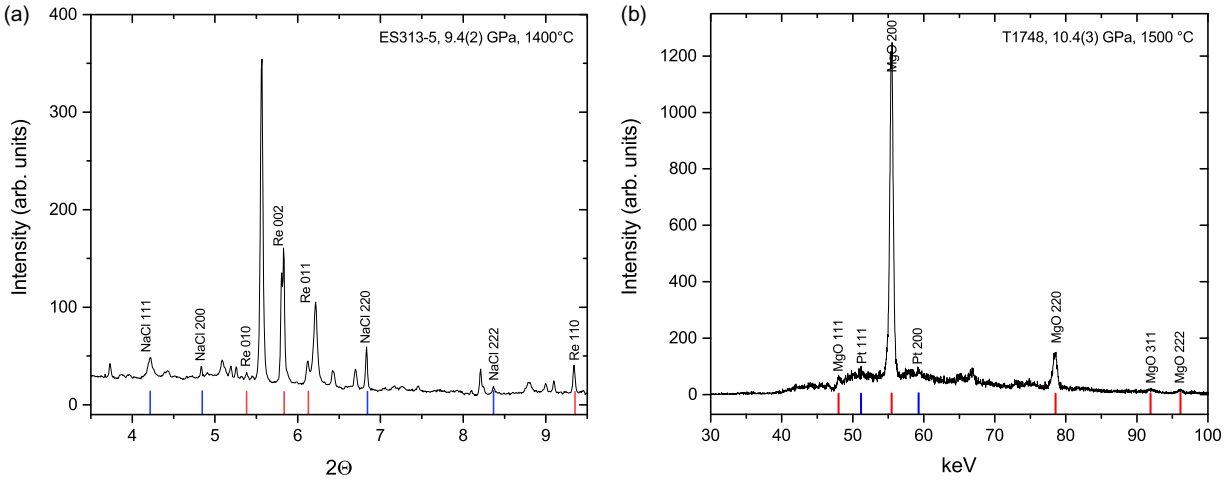

Fig. 3. Representative X-ray diffraction patterns collected in energy dispersive mode at APS (b) and wave-length dispersive modes at ESRF (a). Diffraction peaks of the pressure calibrants are labeled.

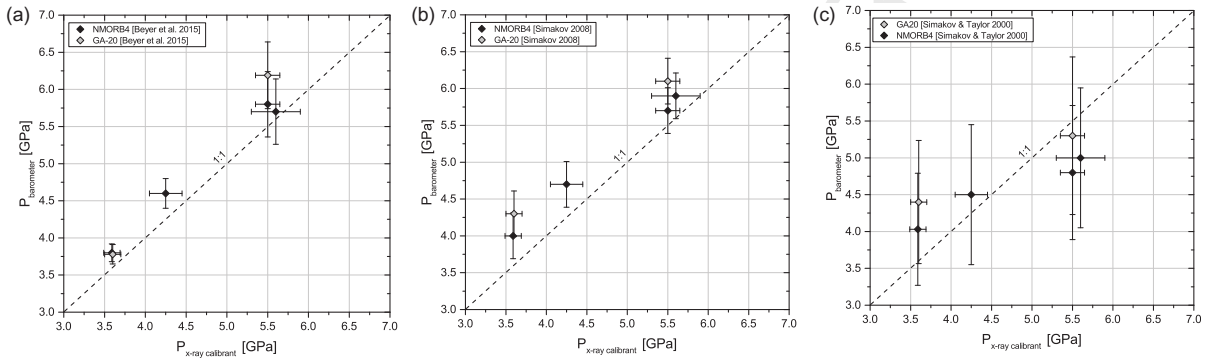

Fig. 4. Calculated pressure vs. experimental pressure for barometers applicable to eclogitic lithologies. The following barometers are shown: (a) B15 (Beyer et al., 2015), (b) S08 (Simakov, 2008), and (c) ST00 (Simakov and Taylor, 2000). Error bars represent the uncertainties of the barometers as given in the original papers and the uncertainties from the volumes of the X-ray calibrants.

ES313-1, the method of extracting pressure and temperature conditions essentially varies input temperatures until the difference between simultaneously calculated pressures, from the unit-cell volumes of Re and h-BN, is minimized, following the scheme outlined in Crichton and Mezouar (2002). For run ES313-1 the Re ambient pressure unit-cell volume has been rescaled by the $d(002)\text{h-BN}_{\text{JCPDS-standard}}$ (3.3318 Å). To verify the robustness of the method, we compared calculated temperatures with measured temperatures where possible. The Re and h-BN method yield temperatures of 1316(28) °C and 1206(18) °C for run ES313-2 and run ES313-4, respectively. This is in reasonable agreement with the thermocouple temperatures as reported in Table 2. We conducted a cross-check of the calculated pressures by using the 3rd order Birch-Murnaghan EoS with the modified Mie-Grüneisen-Debye formulation of Yokoo et al. (2009) for gold. The pressures obtained from the lattice parameters of gold agree with the Re-h-BN pressures within the uncertainties (Supplementary Tables S2 and S3). For the final run ES313-5 we used the unit-cell volume of NaCl to calculate the pressure by applying a fourth-order Birch-Murnaghan EoS with the Mie-Grüneisen expansion for the thermal contribution (Matsui et al., 2012). During the annealing phase at high P and T, corresponding to the periods of time reported in Table 2, pressures varied by less than 0.2 GPa. We used a Pseudo-Voigt function to fit the diffraction peaks, as implemented in PDIndexer. All unit-cell volumes and the corresponding equation of state used to calculate experimental pressures are listed in Supplementary Tables S1–S6. Uncertainties for the X-ray calibration pressures are reported as standard deviation from the mean of all collected diffraction patterns for each run.

3.4. Barometer calibration

Pressures determined using a selection of widely employed barometers, have been tested against pressure calibrations determined with *in situ* means. These barometer equilibria have all been previously calibrated using experiments on either natural starting materials or synthetic materials within realistic natural systems. The chosen equi-

Please cite this article in press as: Beyer C., et al. An internally consistent pressure calibration of geobarometers applicable to the Earth's upper mantle using *in situ* XRD. *Geochim. Cosmochim. Acta* (2017), https://doi.org/10.1016/j.gca.2017.10.031

libria are applicable to a range of compositions, such as fertile and refractory peridotites, eclogites and pyroxenites at Earth's upper mantle conditions.

3.5. Eclogitic barometers

The eclogitic B15 and S08 barometers of Beyer et al. (2015) and Simakov (2008), respectively are based on garnet – clinopyroxene phase equilibria, whereas the ST00 barometer of Simakov and Taylor (2000) solely relies on the solubility of Ca-Tschermaks in clinopyroxene. In Fig. 4 barometric pressures are plotted against the pressure calculated from the EoS of the X-ray calibrants as discussed in the previous section. Within the examined pressure range of 3.6–5.6 GPa the B15 barometer overestimates the experimental pressure by 0.25(5) GPa on average. However, given that the minimum barometer's 2σ uncertainty is 0.4 GPa, which increases with low concentrations of ^{IV}Al (Beyer et al., 2015), the deviation is within the precision of the barometer. Applying the S08 barometer to the same subset of eclogitic samples, experimental pressures are overestimate by 0.46(1) GPa on average, which is slightly larger than the reported precision of 0.31 GPa for the S08 barometer. The ST00 barometer shows a distinct trend that overestimates pressures below ~4.5 GPa and underestimates pressures above 5 GPa. To correct this bias, we fitted a simple linear equation of the form y = a * x + b to the data shown in Fig. 5:

$$\Delta P(ST00)_{corr}\ [\mathrm{GPa}] = 0.58(9) * P - 2.7(5), \quad R^2 = 0.90 \tag{1}$$

If all adjustments are considered, all three barometers yield similar pressures within the compositional range of their original calibration.

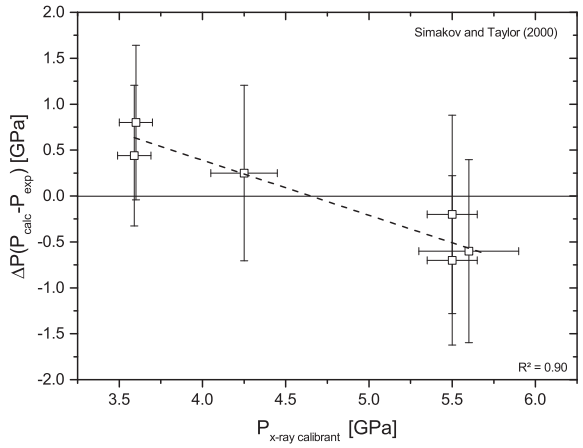

Fig. 5. The difference between the calculated and experimental pressure plotted as a function of the experimental pressure. The linear correction for the ST00 (Simakov and Taylor, 2000) cats-in-cpx barometer is shown by a dashed line. Error bars represent the uncertainties of the barometers as given in the original papers and the uncertainties from the volumes of the X-ray calibrants.

3.6. Peridotitic barometers

The Al-in-orthopyroxene BKN90 (Brey and Köhler, 1990; Brey et al., 1990) and B08 (Brey et al., 2008) barometer, respectively, are depicted in Fig. 6. For the well-known and widely used BKN90 barometer we calculated an average offset of 0.6 GPa between the barometer and the experimental pressure within the examined pressure interval. However, as mentioned in the previous section, some of our experimental samples lost Fe to the $Au_{80}Pd_{20}$ capsules. Although the temperatures calculated with the Ca-in-opx thermometer (Brey and Köhler, 1990) are in very good agreement, the calculated pressures for the Fe-poor samples are systematically higher (Fig. 6, grey symbols). As proposed in the previous section, the slow Al diffusivity resulted in Al concentrations in orthopyroxene that are not reflecting the true equilibrium pressure. The effect of Fe on Al in orthopyroxene is not accounted for in the

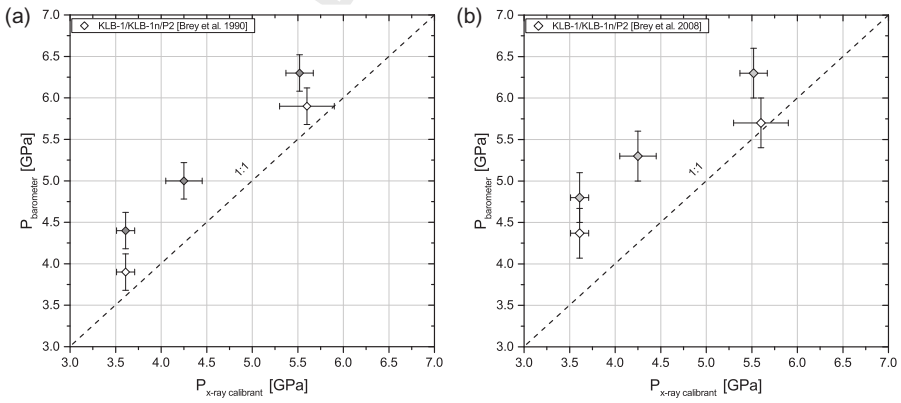

Fig. 6. Calculated pressure vs. experimental pressure for barometers applicable to peridotitic lithologies. The following barometers are shown: (a) BK90 (Brey and Köhler, 1990) and (b) B08 (Brey et al., 2008). Grey symbols mark experiments where Fe-loss occurred which had a consequent influence on the Al-concentration in orthopyroxene. Error bars represent the uncertainties of the barometers as given in the original papers and the uncertainties from the volumes of the X-ray calibrants. Note that the 8 GPa experiment with peridotitic composition was not used, due to the absence of orthopyroxene.

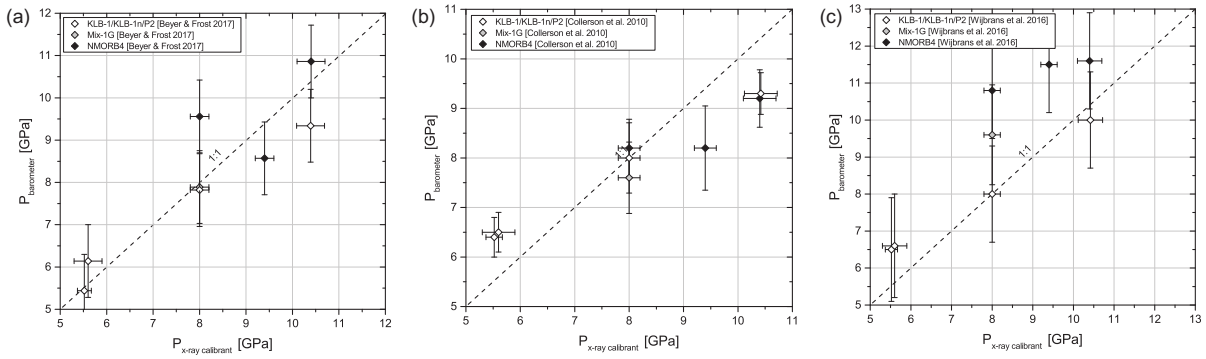

Fig. 7. Calculated pressure vs. experimental pressure for barometers applicable to majoritic garnets. The following barometers are shown: (a) BF17 (Beyer and Frost, 2017), (b) C10 (Collerson et al., 2010) and (c) W16P/W16E (Wijbrans et al., 2016). Error bars represent the uncertainties of the barometers as given in the original papers and the uncertainties from the volumes of the X-ray calibrants.

barometer because it extends outside of the range of the majority of natural samples. The combination of slow Al-diffusion and Fe-dependency leads to a systematic offset of the barometer pressures to values that are higher than the experimental pressures. The most Fe-depleted samples are therefore a poor test of the barometer and are excluded, although still plotted in Fig. 6 as grey symbols. The calculated pressures for the remaining samples (Fig. 6, white symbols) appear to only slightly overestimate the experimental pressure by ~0.3 GPa, which is then very close to the stated uncertainty of 0.22 GPa of the barometer.

The B08 barometer, which is an updated calibration of the BKN90 barometer, reproduces the experimental pressure less accurately with up to 0.8 GPa deviation between calculated and measured pressure. It would appear therefore that the BKN90 barometer provides a better determination of pressures compared to the B08 barometer between 3 and 6 GPa.

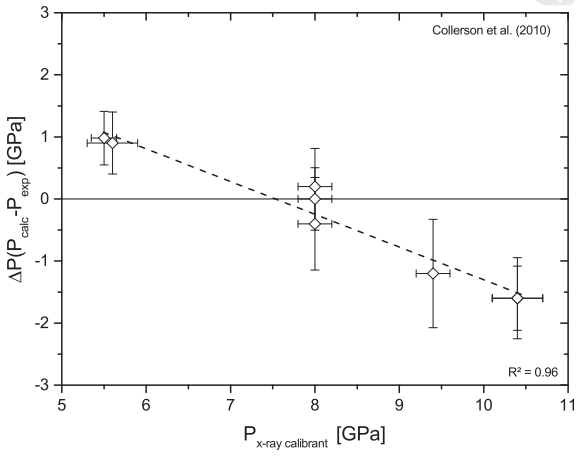

Fig. 8. The difference between the calculated and experimental pressure plotted as a function of experimental pressure for the C10 barometer (Collerson et al., 2010). A linear correction for the C10 barometer is shown as the dashed line. Vertical error bars show the uncertainties in the barometer pressures, as calculated in the original paper and the horizontal uncertainties are from the volumes of the X-ray calibrants.

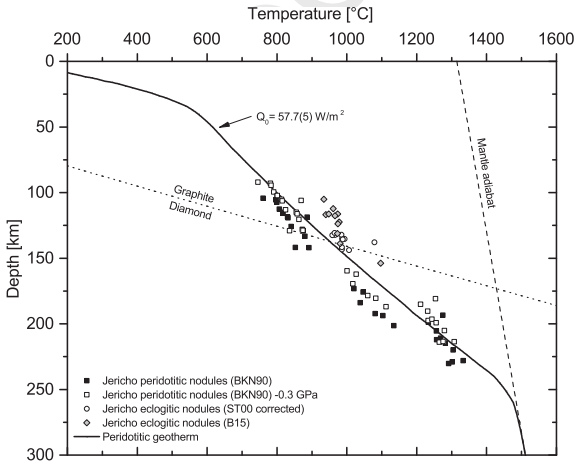

Fig. 9. Experimental pressures calculated with the BKN90 (Brey and Köhler, 1990) barometer for peridotitic xenoliths and B15 (Beyer et al., 2015) and ST00 (Simakov and Taylor, 2000) barometers for the eclogitic xenoliths of the Jericho kimberlite, Slave craton, Canada. Temperature was calculated with the BKN90 geothermometer for peridotites and with the Ellis and Green (1979) [EG79] thermometer for eclogites. The solid black line represents the geotherm fitted to the BKN90 barometer with a minor adjustment of −0.3 GPa to better match the eclogitic xenoliths. Pressure and temperature were fitted using PTQuick. The dashed line represents the graphite/diamond phase boundary (Kennedy and Kennedy, 1976).

3.7. Majoritic barometers

We tested the three currently available majorite barometers BF17 of Beyer and Frost (2017), C10 of Collerson et al. (2010), and W16 of Wijbrans et al. (2016) at pressures ranging from 5.5 to 10.4 GPa, i.e. from cratonic (sub)lithospheric mantle depths to depths, reaching lowermost upper mantle conditions above Earth's transition zone. Calculated pressures are shown in Fig. 7. The BF17 barometer reproduces the experimental pressures to within $1\sigma = 0.17$ GPa (Fig. 7a). Calculated pressures are well within the barometer's precision of 0.86 GPa, except for one outlier at 8 GPa with $\Delta P = +1.4$ GPa. We observed no systematic over- or underestimation of experimental pressures.

Please cite this article in press as: Beyer C., et al. An internally consistent pressure calibration of geobarometers applicable to the Earth's upper mantle using *in situ* XRD. *Geochim. Cosmochim. Acta* (2017), https://doi.org/10.1016/j.gca.2017.10.031

The C10 barometer produces a systematic trend from overestimating pressures below 7 GPa up to 1 GPa and underestimating pressures above 9 GPa up to −1.5 GPa. This behavior produces an artificial normalization of pressures around 8 GPa (Fig. 7b). Never the less, the bias can be easily corrected by applying a linear correction as employed for the ST00 barometer. Fitting the C10 pressures to the linear expression, with propagation of the uncertainties of the barometer and the X-ray calibrant volumes, yields:

$$\Delta P(C10)_{corr}\ [\mathrm{GPa}] = 0.52(4) * P(C10) - 3.9(3), \quad R^2 = 0.96 \qquad (2)$$

The linear fit is shown in Fig. 8. Although we have not performed experiments above 10.4 GPa, we assume monotonic behavior for the C10 barometer linear correction on the basis of previous findings up to 16 GPa for eclogitic and pyroxenitic majoritic garnets (Fig. 6 in Beyer and Frost, 2017). For peridotitic compositions the correction factor should be only applied up to ~11 GPa (see Fig. 9).

Wijbrans et al. (2016) provided two distinct equations to fit eclogites and peridotites individually. We found that the peridotitic formulation (W16P) reproduces the experimental pressures better than 1 GPa on average, hence, a correction is not necessary (Fig. 7c). The equation for the eclogitic compositions (W16E) reproduces experimental pressures less well but there is no systematic offset that can be corrected (Fig. 7c).

That is, as demonstrated above, three barometers for peridotitic compositions (BF17, C10, W16P) and two barometers for eclogitic, and pyroxenitic compositions (BF17, C10) yield consistent pressures after applying corrections, within their expected uncertainties, and are thus suitable to determine the depth of last equilibration of majoritic garnet inclusions in diamonds.

3.8. Application

We applied the Brey and Köhler (1990) barometer to a suite of undisturbed peridotites from the Jericho kimberlite, Slave Craton (Kopylova et al., 1999) and compared the modeled peridotitic geotherm to the pressure and temperature estimated from eclogitic nodules from the Jericho kimberlite (De Stefano et al., 2009). Pressures and temperatures of eclogitic garnet-clinopyroxene pairs in diamonds were obtained by using of the Beyer et al. (2015) geobarometer with the Ellis and Green (1979) geothermometer, calculated iteratively with the software PTQuick (http://www.dimadd.ru/en/Programs/ptquick). Furthermore, we also compare the results of using the corrected Simakov and Taylor (2000) barometer on the same samples. We made use of the model of McKenzie et al. (2005) to calculate the steady state geotherm. We find that by making a very small correction of −0.3 GPa for the BKN90 barometer the steady-state conductive geotherm is shifted towards higher surface heat flow (56.7(8) mW/m^2 to 57.7(5) mW/m^2), which moves the peridotite data into slightly better agreement with the eclogites. The geotherm has been obtained by using values for thermal conductivity (K = 2.5 W/K m) and heat generation rate (H = 1.12 μW/m^3) as used by McKenzie et al. (2005). We found that the updated geotherm of the peridotites is larger by ~3 mW/m^2 than surface heat flow measurements of the Slave Craton of 53.3–54.4 mW/m^2 and 54.4(4) mW/m^2 (Beck and Sass, 1966; Lewis and Wang, 1992). This could have multiple implications, either the lithosphere is very thick with ~260 km but could also indicate a lower mantle potential temperature. Since the thermal gradient at the base of the mechanical boundary layer is about 4 K/km, a 100 K decrease in mantle temperature would equate to a 25 km thinner lithosphere using the same model parameters. Moreover, the best fit model indicates that the radiogenic output of the crust is higher than previous estimates (McKenzie et al., 2005).

Applying the B15 barometer to the eclogitic nodules returns depth of 105–154 km, whereas, the same set of xenoliths calculated with the ST00 barometer is shifted to slightly greater depths and locates the eclogitic suite in a narrower depth interval of 130–145 km. Both geobarometers put the eclogitic xenoliths close to the diamond stability field within the uncertainties of pressure and temperature.

Our new estimates, both on peridotites and eclogites, support previous findings that the area around the Jericho kimberlite was exposed to an unusually high radiogenic environment (Kopylova et al., 1999).

Samples from the Juina kimberlite field, Sao Luiz, Brazil, have attracted significant attention in recent years (Kaminsky et al., 2001; Walter et al., 2011; Thomson et al., 2014; Zedgenizov et al., 2015) because "sub-lithospheric" mineral inclusions in these diamonds have been identified. These inclusions comprise minerals that certainly originated from the transition zone (majoritic garnet) and possibly the lower mantle (bridgmanite, $CaSiO_3$-perovskite, ferropericlase, TAPP). It is very important to be able to identify their depth of formation to develop a comprehensive understanding of the state of Earth's deep interior and in particular carbon mobility processes. Hence,

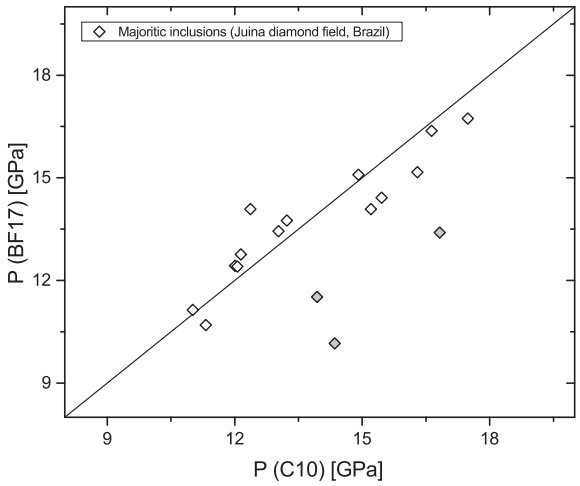

Fig. 10. Pressure calculated with the BF17 (Beyer and Frost, 2017) and the corrected C10 (Collerson et al., 2010) barometer of majoritic garnet inclusions from Juina diamond field, Sao Luiz, Brazil. The grey symbols represent inclusions from sample 5–108 that have a high concentration of TiO_2 as discussed in the text.

Please cite this article in press as: Beyer C., et al. An internally consistent pressure calibration of geobarometers applicable to the Earth's upper mantle using *in situ* XRD. *Geochim. Cosmochim. Acta* (2017), https://doi.org/10.1016/j.gca.2017.10.031

Table 5
Correction factors for geobarometers.

Barometer	Correction factor (ΔP) [GPa]	Reference
S08	−0.46(1)	Simakov (2008)
ST00	0.58(9) * P_{ST00} − 2.7(5)	Simakov and Taylor (2000)
C10	0.52(4) * P_{C10} − 3.9(3)	Collerson et al. (2010)

we applied the BF17 and C10 barometer to a set of inclusions with majoritic garnets. The updated C10 barometer is in very good agreement with the BF17 barometer within the uncertainties (Fig. 10). However, as can be seen in Fig. 10 several outliers still exist, which in these cases arise from a single diamond, 5–108, (Kaminsky et al., 2001) that contains three majoritic garnets that each have high TiO_2 contents of ~2 wt.%. This indicates that the effect of Ti, which cannot be unambiguously attributed to the majorite type substitution (Huggins et al., 1977), is potentially not well constrained at these concentrations by either model.

4. CONCLUSIONS

On the basis of our results, it is apparent that a direct calibration of geobarometers is important for refining the precision and internal consistency of obtained pressures. Systematic errors between barometer pressure and temperature corrections have been minimized by our experimental approach, in which various mantle lithologies equilibrated in multi-chamber runs at similar pressure and temperature conditions. The consistent data set obtained ensures the comparability between determined pressures for geobarometers previously established for peridotites and eclogites.

Moreover, the application of our pressure corrections to these widely used barometers allows the determination of the latest equilibration conditions of eclogites and peridotites from the same rock suite as exemplified for xenoliths from the Jericho kimberlite. With the corrections presented in this study we can rule out inconsistencies that were inevitable due to different pressure calibrations between different laboratories. The herein obtained correction factors are summarized in Table 5.

However, we emphasize that xenoliths with bulk compositions that are markedly different from the original barometer calibrations might still yield ambiguous pressures. A potential problem may exist because certain components remain unquantified in some barometer models, such as the effect of Fe^{3+}-bearing end-members for example or the onset of phase-transitions, such as ordering in omphacite, which could have distinct effects on the calculations under conditions where these end-members or transitions are dominant. For very oxidized assemblages Fe^{3+} may have a significant effect on the iterative calculation of pressure and temperature, particularly when the barometers are combined with garnet – orthopyroxene thermometers, whereas, the effect on garnet – olivine and garnet – clinopyroxene thermometers will be small (Purwin et al., 2013; Matjuschkin et al., 2014; Nimis et al., 2015).

Nevertheless, certainly for higher pressure barometers such as that based on majoritic garnet uncertainties likely still exists arising from poorly constrained influences of e.g. Fe^{3+}, Cr^{3+} and Ti^{4+} and potentially also volatiles that are not normally characterized.

ACKNOWLEDGMENTS

This study has been funded by the DFG Grant no. FR1555-9. C.B. would like to thank J. Berndt for providing uncomplicated and fast access to the microprobe at the Westfälische Wilhelms-Universität Münster. A.R. acknowledges funding by an Auvergne Postdoctoral Research Fellowship. Support to A.R. from Prof. S. W. Faryad (GAČR-project#: 242-201209) is also greatly appreciated. We thank the APS and ESRF for access to beamtime, through proposals 42985 and ES-313, respectively. This research used resources of the Advanced Photon Source, a U.S. Department of Energy (DOE) Office of Science User Facility operated for the DOE Office of Science by Argonne National Laboratory under Contract No. DE-AC02-06CH11357. We thank G. Yaxley and one anonymous reviewer for their comments that helped to improve the manuscript.

APPENDIX A. SUPPLEMENTARY MATERIAL

Supplementary data associated with this article can be found, in the online version, at https://doi.org/10.1016/j.gca.2017.10.031.

REFERENCES

Ashchepkov I. V. et al. (2010) Structure and evolution of the lithospheric mantle beneath Siberian craton, thermobarometric study. *Tectonophysics* **485**, 17–41.

Beck A. and Sass J. (1966) A preliminary value of heat flow at the Muskox Intrusion near Coppermine, NWT, Canada. *Earth Planet. Sci. Lett.* **1**, 123–129.

Beyer C. and Frost D. J. (2017) The depth of sub-lithospheric diamond formation and the redistribution of carbon in the deep mantle. *Earth Planet. Sci. Lett.* **461**, 30–39. https://doi.org/10.1016/j.epsl.2016.12.017.

Beyer C., Frost D. J. and Miyajima N. (2015) Experimental calibration of a garnet–clinopyroxene geobarometer for mantle eclogites. *Contrib. Mineral. Petrol.* **169**, 1–21. https://doi.org/10.1007/s00410-015-1113-z.

Bohlen S. R. and Boettcher A. L. (1982) The quartz ⇆ coesite transformation: a precise determination and the effects of other components. *J. Geophys. Res. Solid Earth* **87**, 7073–7078. https://doi.org/10.1029/JB087iB08p07073.

Bose K. and Ganguly J. (1995) Experimental and theoretical studies of the stabilities of talc, antigorite and phase A at high pressures with applications to subduction processes. *Earth Planet. Sci. Lett.* **136**, 109–121.

Brey G. and Köhler T. (1990) Geothermobarometry in four-phase lherzolites II. New thermobarometers, and practical assessment of existing thermobarometers. *J. Pet. Geol.* **31**, 1353–1378.

Brey G. P., Bulatov V. K. and Girnis A. V. (2008) Geobarometry for peridotites: experiments in simple and natural systems from 6 to 10 GPa. *J. Pet. Geol.* **49**, 3–24.

Brey G. P., Köhler T. and Nickel K. G. (1990) Geothermobarometry in four-phase lherzolites I. Experimental results from 10 to 60 kb. *J. Pet. Geol.* **31**, 1313–1352. https://doi.org/10.1093/petrology/31.6.1313.

Collerson K. D., Williams Q., Kamber B. S., Omori S., Arai H. and Ohtani E. (2010) Majoritic garnet: a new approach to pressure estimation of shock events in meteorites and the encapsulation of sub-lithospheric inclusions in diamond. *Geochim. Cosmochim. Acta* **74**, 5939–5957.

Crichton W. A. and Mezouar M. (2002) Noninvasive pressure and temperature estimation in large-volume apparatus by equation-of-state cross-calibration. *High Temp. High Press.* **34**, 235–242.

Dale J. and Holland T. (2003) Geothermobarometry, P-T paths and metamorphic field gradients of high-pressure rocks from the Adula Nappe, Central Alps. *J. Metam. Geol.* **21**, 813–829.

De Stefano A., Kopylova M. G., Cartigny P. and Afanasiev V. (2009) Diamonds and eclogites of the Jericho kimberlite (Northern Canada). *Contrib. Mineral. Petrol.* **158**, 295–315. https://doi.org/10.1007/s00410-009-0384-7.

Ellis D. J. and Green D. H. (1979) An experimental study of the effect of Ca upon garnet-clinopyroxene Fe-Mg exchange equilibria. *Contrib. Mineral. Petrol.* **71**, 13–22. https://doi.org/10.1007/bf00371878.

Getting I. and Kennedy G. (1970) Effect of pressure on the emf of chromel-alumel and platinum-platinum 10% rhodium thermocouples. *J. Appl. Phys.* **41**, 4552–4562.

Green D. H., Hibberson W. O., Kovács I. and Rosenthal A. (2010) Water and its influence on the lithosphere-asthenosphere boundary. *Nature* **467**, 448–451.

Hammersley A. (2016) FIT2D: a multi-purpose data reduction, analysis and visualization program. *J. Appl. Crystallogr.* **49**, 646–652.

Hirschmann M. M., Aubaud C. and Withers A. C. (2005) Storage capacity of H_2O in nominally anhydrous minerals in the upper mantle. *Earth Planet. Sci. Lett.* **236**, 167–181.

Hirschmann M. M., Kogiso T., Baker M. B. and Stolper E. M. (2003) Alkalic magmas generated by partial melting of garnet pyroxenite. *Geology* **31**, 481–484.

Holloway J. R. and Wood B. J. (2012) *Simulating the Earth: Experimental Geochemistry*. Springer.

Huggins F., Virgo D. and Huckenholz H. (1977) Titanium-containing silicate garnet; I, The distribution of Al, Fe (super 3+), and Ti (super 4+) between octahedral and tetrahedral sites. *Am. Miner.* **62**, 475–490.

Irifune T., Sekine T., Ringwood A. E. and Hibberson W. O. (1986) The eclogite-garnetite transformation at high pressure and some geophysical implications. *Earth Planet. Sci. Lett.* **77**, 245–256. https://doi.org/10.1016/0012-821x(86)90165-2.

Kaminsky F., Zakharchenko O., Davies R., Griffin W., Khachatryan-Blinova G. and Shiryaev A. (2001) Superdeep diamonds from the Juina area, Mato Grosso State, Brazil. *Contrib. Mineral. Petrol.* **140**, 734–753.

Katayama I., Hirose K., Yurimoto H. and Nakashima S. (2003) Water solubility in majoritic garnet in subducting oceanic crust. *Geophys. Res. Lett.* **30**. https://doi.org/10.1029/2003gl018127.

Kennedy C. S. and Kennedy G. C. (1976) The equilibrium boundary between graphite and diamond. *J. Geophys. Res.* **81**, 2467–2470.

Keppler H. and Frost D. J. (2005) Introduction to minerals under extreme conditions. *Miner. Behav. Extreme Cond. EMU Notes Miner.* **7**, 1–30.

Kopylova M., Russell J. and Cookenboo H. (1999) Petrology of peridotite and pyroxenite xenoliths from the Jericho kimberlite: implications for the thermal state of the mantle beneath the Slave craton, northern Canada. *J. Pet. Geol.* **40**, 79–104.

Le Godec Y, Martinez-Garcia D, Mezouar M, Syfosse G, Itie J, Besson J. (2000). Equation of state and order parameter in graphite-like h-BN under high pressure and temperature. In: *Proceedings of AIRAPT-17: Science and Technology of High Pressure*. pp. 925–928.

Lee H. Y. and Ganguly J. (1988) Equilibrium compositions of coexisting garnet and orthopyroxene: experimental determinations in the system FeO-MgO-Al2O3-SiO2, and applications. *J. Pet. Geol.* **29**, 93–113.

Lewis T. J. and Wang K. (1992) Influence of terrain on bedrock temperatures. *Palaeogeogr. Palaeoclimatol. Palaeoecol.* **98**, 87–100.

Liebske C. and Frost D. J. (2012) Melting phase relations in the MgO–MgSiO3 system between 16 and 26 GPa: Implications for melting in Earth's deep interior. *Earth Planet. Sci. Lett.* **345–348**, 159–170. https://doi.org/10.1016/j.epsl.2012.06.038.

Matjuschkin V., Brey G. P., Höfer H. E. and Woodland A. B. (2014) The influence of Fe3+ on garnet–orthopyroxene and garnet–olivine geothermometers. *Contrib. Mineral. Petrol.* **167**, 972. https://doi.org/10.1007/s00410-014-0972-z.

Matsui M., Higo Y., Okamoto Y., Irifune T. and Funakoshi K.-I. (2012) Simultaneous sound velocity and density measurements of NaCl at high temperatures and pressures: application as a primary pressure standard. *Am. Miner.* **97**, 1670–1675.

McKenzie D., Jackson J. and Priestley K. (2005) Thermal structure of oceanic and continental lithosphere. *Earth Planet. Sci. Lett.* **233**, 337–349.

Morard G. et al. (2007) Optimization of Paris-Edinburgh press cell assemblies for in situ monochromatic X-ray diffraction and X-ray absorption. *High Press. Res.* **27**, 223–233.

Myhill R., Frost D. J. and Novella D. (2017) Hydrous melting and partitioning in and above the mantle transition zone: insights from water-rich MgO–SiO2–H2O experiments. *Geochim. Cosmochim. Acta* **200**, 408–421. https://doi.org/10.1016/j.gca.2016.05.027.

Nimis P., Goncharov A., Ionov D. A. and McCammon C. (2015) Fe3+ partitioning systematics between orthopyroxene and garnet in mantle peridotite xenoliths and implications for thermobarometry of oxidized and reduced mantle rocks. *Contrib. Mineral. Petrol.* **169**, 1–18.

Purwin H., Lauterbach S., Brey G. P., Woodland A. B. and Kleebe H.-J. (2013) An experimental study of the Fe oxidation states in garnet and clinopyroxene as a function of temperature in the system $CaO–FeO–Fe_2O_3–MgO–Al_2O_3–SiO_2$: implications for garnet–clinopyroxene geothermometry. *Contrib. Mineral. Petrol.*, 1–17.

Rosenthal A., Hauri E. H. and Hirschmann M. M. (2015) Experimental determination of C, F and H partitioning between mantle minerals and carbonated basalt, CO_2/Ba and CO_2/Nb systematics of partial melting, and the CO_2 contents of basaltic source regions. *Earth Planet. Sci. Lett.* **412**, 77–87. https://doi.org/10.1016/j.epsl.2014.11.044.

Rosenthal A., Yaxley G. M., Green D. H., Hermann J., Kovacs I. and Spandler C. (2014) Continuous eclogite melting and variable refertilisation in upwelling heterogeneous mantle. *Sci. Rep.* **4**, 6099. https://doi.org/10.1038/srep06099.

Rubie D. C. (1999) Characterising the sample environment in multianvil high-pressure experiments. *Phase Transit.* **68**, 431–451. https://doi.org/10.1080/01411599908224526.

Seto Y., Nishio-Hamane D., Nagai T. and Sata N. (2010) Development of a software suite on X-ray diffraction experiments. *Rev. High Press. Sci. Technol.* **20**, 269–276.

Shirey S. B. et al. (2001) Archean emplacement of eclogitic components into the lithospheric mantle during formation of

Please cite this article in press as: Beyer C., et al. An internally consistent pressure calibration of geobarometers applicable to the Earth's upper mantle using *in situ* XRD. *Geochim. Cosmochim. Acta* (2017), https://doi.org/10.1016/j.gca.2017.10.031

the Kaapvaal Craton. *Geophys. Res. Lett.* **28**, 2509–2512. https://doi.org/10.1029/2000GL012589.

Simakov S. K. (2008) Garnet–clinopyroxene and clinopyroxene geothermobarometry of deep mantle and crust eclogites and peridotites. *Lithos* **106**, 125–136. https://doi.org/10.1016/j.lithos.2008.06.01.

Simakov S. K. and Taylor L. A. (2000) Geobarometry for mantle eclogites: solubility of Ca-Tschermaks in clinopyroxene. *Int. Geol. Rev.* **42**, 534–544.

Smart K. A., Heaman L. M., Chacko T., Simonetti A., Kopylova M., Mah D. and Daniels D. (2009) The origin of high-MgO diamond eclogites from the Jericho Kimberlite, Canada. *Earth Planet. Sci. Lett.* **284**, 527–537.

Smith D. and Barron B. R. (1991) Pyroxene-garnet equilibration during cooling in the mantle. *Am. Miner.* **76**, 1950–1963.

Sokolova T. S., Dorogokupets P. I., Dymshits A. M., Danilov B. S. and Litasov K. D. (2016) Microsoft excel spreadsheets for calculation of P-V–T relations and thermodynamic properties from equations of state of MgO, diamond and nine metals as pressure markers in high-pressure and high-temperature experiments. *Comput. Geosci.* **94**, 162–169. https://doi.org/10.1016/j.cageo.2016.06.002.

Spandler C., Yaxley G., Green D. H. and Rosenthal A. (2008) Phase relations and melting of anhydrous K-bearing eclogite from 1200 to 1600 C and 3 to 5 GPa. *J. Pet. Geol.* **49**, 771–795.

Takahashi E. (1986) Melting of a dry peridotite KLB-1 up to 14 GPa: implications on the origin of peridotitic upper mantle. *J. Geophys. Res. Solid Earth* **91**, 9367–9382.

Tange Y., Nishihara Y. and Tsuchiya T. (2009) Unified analyses for P-V-T equation of state of MgO: a solution for pressure-scale problems in high P-T experiments. *J. Geophys. Res. Solid Earth* **114**.

Thomson A. R., Kohn S. C., Bulanova G. P., Smith C. B., Araujo D. and Walter M. J. (2014) Origin of sub-lithospheric diamonds from the Juina-5 kimberlite (Brazil): constraints from carbon isotopes and inclusion compositions. *Contrib. Mineral. Petrol.* **168**, 1–29. https://doi.org/10.1007/s00410-014-1081-8.

Walter M. J. (1998) Melting of garnet peridotite and the origin of komatiite and depleted lithosphere. *J. Pet. Geol.* **39**, 29–60. https://doi.org/10.1093/petroj/39.1.29.

Walter M. J. et al. (2011) Deep mantle cycling of oceanic crust: evidence from diamonds and their mineral inclusions. *Science* **334**, 54–57. https://doi.org/10.1126/science.1209300.

Wang Y. B., Rivers M., Sutton S., Nishiyama N., Uchida T. and Sanehira T. (2009) The large-volume high-pressure facility at GSECARS: a "Swiss-army-knife" approach to synchrotron-based experimental studies. *Phys. Earth Planet. Inter.* **174**, 270–281. https://doi.org/10.1016/j.pepi.2008.06.01.

Wijbrans C. H., Rohrbach A. and Klemme S. (2016) An experimental investigation of the stability of majoritic garnet in the Earth's mantle and an improved majorite geobarometer. *Contrib. Mineral. Petrol.* **171**, 1–20. https://doi.org/10.1007/s00410-016-1255-7.

Yokoo M., Kawai N., Nakamura K. G., Kondo K.-I., Tange Y. and Tsuchiya T. (2009) Ultrahigh-pressure scales for gold and platinum at pressures up to 550 GPa. *Phys. Rev. B* **80**, 104114.

Zedgenizov D., Shatsky V., Panin A., Evtushenko O., Ragozin A. and Kagi H. (2015) Evidence for phase transitions in mineral inclusions in superdeep diamonds of the Sao Luiz deposit (Brazil). *Russ. Geol. Geophys.* **56**, 296–305.

Zha C.-S., Bassett W. A. and Shim S.-H. (2004) Rhenium, an in situ pressure calibrant for internally heated diamond anvil cells. *Rev. Sci. Instrum.* **75**, 2409–2418.

Associate editor: Andrew J. Campbell